BROMI/TBC1D32 together with CCRK/CDK20 and FAM149B1/JBTS36 contributes to intraflagellar transport turnaround involving ICK/CILK1

Yuuki Satoda†, Tatsuro Noguchi†, Taiju Fujii, Aoi Taniguchi, Yohei Katoh*, and Kazuhisa Nakayama*
Department of Physiological Chemistry, Graduate School of Pharmaceutical Sciences, Kyoto University, Sakyo-ku, Kyoto 606-8501, Japan

ABSTRACT **Primary cilia are antenna-like organelles that contain specific proteins, and are crucial for tissue morphogenesis. Anterograde and retrograde trafficking of ciliary proteins are mediated by the intraflagellar transport (IFT) machinery. BROMI/TBC1D32 interacts with CCRK/CDK20, which phosphorylates and activates the intestinal cell kinase (ICK)/CILK1 kinase, to regulate the change in direction of the IFT machinery at the ciliary tip. Mutations in *BROMI*, *CCRK*, and *ICK* in humans cause ciliopathies, and mice defective in these genes are also known to demonstrate ciliopathy phenotypes. We show here that BROMI interacts not only with CCRK but also with CFAP20, an evolutionarily conserved ciliary protein, and with FAM149B1/ Joubert syndrome (JBTS)36, a protein in which mutations cause JBTS. In addition, we show that FAM149B1 interacts directly with CCRK as well as with BROMI. Ciliary defects observed in *CCRK*-knockout (KO), *BROMI*-KO, and *FAM149B1*-KO cells, including abnormally long cilia and accumulation of the IFT machinery and ICK at the ciliary tip, resembled one another, and BROMI mutants that are defective in binding to CCRK and CFAP20 were unable to rescue the ciliary defects of *BROMI*-KO cells. These data indicate that CCRK, BROMI, FAM149B1, and probably CFAP20 altogether regulate the IFT turnaround process under the control of ICK.**

Monitoring Editor
Guangshuo Ou
Tsinghua University

Received: Mar 10, 2022
Revised: May 11, 2022
Accepted: May 20, 2022

INTRODUCTION

A variety of eukaryotic cell types use primary cilia as cellular antennae to sense and transduce mechanical signals, such as fluid flow, and biochemical signals, such as the Hedgehog (Hh) family of morphogens (Nachury and Mick, 2019; Kopinke *et al.*, 2021). To fulfill these functions, there are specific receptors and ion channels on the ciliary membrane. The membrane and interior of cilia are distinguished from the plasma membrane and cytoplasm, respectively, by the presence of the ciliary gate comprising transition fibers and the transition zone (TZ), which together act as a permeability/diffusion barrier (Garcia-Gonzalo and Reiter, 2017; Nachury and Mick, 2019). Not only bidirectional protein trafficking along the axonemal microtubules within cilia but also import and export of ciliary proteins across the ciliary gate are mediated by a large supramolecular complex called the intraflagellar transport (IFT) machinery

This article was published online ahead of print in MBoC in Press (http://www.molbiolcell.org/cgi/doi/10.1091/mbc.E22-03-0089) on May 24, 2022.

†These authors contributed equally to this study.

Author contributions: Y.S. and T.N. designed and performed the experiments; T.F. and A.T. performed the experiments; and Y.K. and K.N. designed the experiments and prepared the manuscript.

Conflicts of interest: The authors declare that they have no conflicts of interest associated with this study.

*Address correspondence to: Kazuhisa Nakayama (kazunaka@pharm.kyoto-u.ac.jp); Yohei Katoh (ykatoh@pharm.kyoto-u.ac.jp).

Abbreviations used: BBS, Bardet-Biedl syndrome; CCRK, cell cycle-related kinase; DUF, domain of unknown function; ECV, extracellular vesicle; FBS, fetal bovine serum; GFP, green fluorescent protein; GST, glutathione *S*-transferase; Hh, Hedgehog; ICK, intestinal cell kinase; hTERT-RPE1, human telomerase reverse transcriptase-immortalized retinal pigment epithelial 1; IFT, intraflagellar transport; JBTS, Joubert syndrome; KO, knockout; MAK, male germ cell-associated kinase; mChe, mCherry; Nb, nanobody; ROI, region of interest; SAG, Smoothened Agonist; sgRNA, single-guide RNA; SMO, Smoothened; tBFP, TagBFP; TZ, transition zone; WT, wild type.

(Taschner and Lorentzen, 2016; Nakayama and Katoh, 2020). Owing to the crucial roles of primary cilia in embryonic development and tissue homeostasis, mutations in the genes encoding components of the IFT machinery and the TZ result in a large heterogeneous group of disorders, collectively termed the ciliopathies, which include Bardet-Biedl syndrome (BBS) and Joubert syndrome (JBTS) (Braun and Hildebrandt, 2017; Reiter and Leroux, 2017).

The main components of the IFT machinery, often referred to as IFT trains, are the IFT-A and IFT-B complexes (Taschner and Lorentzen, 2016; Nakayama and Katoh, 2020). The IFT-B complex is composed of 16 subunits and mediates the anterograde (from ciliary base to tip) trafficking of proteins powered by the heterotrimeric kinesin-II motor, whereas the heterohexameric IFT-A complex mediates retrograde trafficking powered by the dynein-2 complex (also known as IFT dynein). In addition to these roles in intraciliary trafficking, the IFT-A complex together with the TULP3 adaptor protein mediates the import of membrane proteins across the TZ (Mukhopadhyay *et al.*, 2010; Badgandi *et al.*, 2017; Hirano *et al.*, 2017; Han *et al.*, 2019; Picariello *et al.*, 2019; Kobayashi *et al.*, 2021), whereas the IFT-B complex in conjunction with the BBSome, which is composed of eight BBS proteins, mediates the removal of membrane proteins from cilia (Liu and Lechtreck, 2018; Nozaki *et al.*, 2018; Ye *et al.*, 2018; Nozaki *et al.*, 2019; Liu *et al.*, 2021).

The anterograde and retrograde trafficking along the axonemal microtubules entails the change in IFT direction at the ciliary tip. The turnaround process includes the remodeling of IFT trains, switching of the motor from kinesin to dynein, and loading of retrograde cargoes (Nakayama and Katoh, 2020). Consistent with this notion, cryoelectron tomographic studies revealed that *Chlamydomonas* anterograde and retrograde IFT trains are distinct in size and configuration (Stepanek and Pigino, 2016; Jordan *et al.*, 2018), and a cryoelectron microscopic study suggested that the human dynein-2 complex is transported as an inactive anterograde cargo (Toropova *et al.*, 2019). In addition, mixing of components of the IFT-A and IFT-B complexes at the tip was suggested by live-imaging analyses of the IFT trains moving in flagella/cilia of *Chlamydomonas*, *Caenorhabditis elegans*, and *Trypanosoma brucei* (Chien *et al.*, 2017; Bertiaux *et al.*, 2018; Mijalkovic *et al.*, 2018). However, recent studies in *Chlamydomonas* flagella suggested that a conversion of anterograde to retrograde trains does not involve considerable remodeling at the tip (Wingfield *et al.*, 2021), and that the machinery at the ciliary tip is not always required for the turnaround event (Nievergelt *et al.*, 2021).

One of the key regulators of the turnaround process is intestinal cell kinase (ICK; recently renamed as CILK1) (Fu *et al.*, 2019; Chaya and Furukawa, 2021). ICK and its tissue-specific paralog, male germ cell-associated kinase (MAK), are remote members of the MAP kinase superfamily that contain a canonical TXY motif in the activation loop and localize at the ciliary tips by being transported via binding to the IFT-B complex (Omori *et al.*, 2010; Chaya *et al.*, 2014; Nakamura *et al.*, 2020). ICK mutations in humans cause ciliopathies (Lahiry *et al.*, 2009; Oud *et al.*, 2016; Taylor *et al.*, 2016), and *Ick* mutant mice demonstrate ciliopathy-like phenotypes (Chaya *et al.*, 2014; Moon *et al.*, 2014; Ding *et al.*, 2018). As the kinase activity of ICK is essential for its function (Chaya *et al.*, 2014; Nakamura *et al.*, 2020), the phosphorylation of some substrates by ICK is thought to be crucial for the turnaround process. KIF3A, a motor subunit of heterotrimeric kinesin-II, was proposed to be a candidate substrate of ICK in previous studies (Chaya *et al.*, 2014; Oh *et al.*, 2019), but a recent study suggested that KIF3A phosphorylation is not important for ciliary function (Gailey *et al.*, 2021). On the other hand, it has recently been shown that a phosphomimetic mutant of a *C. elegans* ICK orthologue can phosphorylate the IFT-B subunit IFT74 (Li *et al.*, 2021).

Another kinase, cell cycle-related kinase (CCRK, also known as CDK20), was shown to phosphorylate ICK at the TXY motif (Fu *et al.*, 2005; Fu *et al.*, 2006), and in a *Chlamydomonas* strain defective in a CCRK orthologue (LF2), it was shown that a MAPK-related kinase (LF4) homologous to MOK/ICK/MAK does not undergo phosphorylation (Wang *et al.*, 2019). Consistent with the role of ICK downstream of CCRK, mutations of ICK and CCRK homologues in various organisms cause a long cilia/flagella phenotype and often increase the variation in the ciliary length of individual cells (Asleson and Lefebvre, 1998; Berman *et al.*, 2003; Bengs *et al.*, 2005; Burghoorn *et al.*, 2007; Tam *et al.*, 2007; Omori *et al.*, 2010; Yang *et al.*, 2013; Moon *et al.*, 2014; Okamoto *et al.*, 2017; Yi *et al.*, 2018; Jiang *et al.*, 2019; Maurya *et al.*, 2019; Wang *et al.*, 2019; Nakamura *et al.*, 2020). Furthermore, mutations of CCRK and BROMI (also known as TBC1D32), which interact with CCRK (Ko *et al.*, 2010; Noguchi *et al.*, 2021), in humans cause ciliopathies, and CCRK and BROMI mutant mice demonstrate defects in embryonic development caused by aberrant Hh signaling (Ko *et al.*, 2010; Adly *et al.*, 2014; Snouffer *et al.*, 2017; Wang *et al.*, 2018; Alsahan and Alkuraya, 2020; Hietamäki *et al.*, 2020). We have recently shown that not only in *ICK*-knockout (KO) cells but also in *CCRK*-KO cells derived from human telomerase reverse transcriptase-immortalized retinal pigment epithelial 1 (hTERT-RPE1) cells, the average ciliary length is longer and the variation in ciliary length is larger than in control RPE1 cells, and that excessively accumulated proteins at the bulged ciliary tips of these KO cells are eliminated via extracellular vesicles (ECVs) (Noguchi *et al.*, 2021). It is interesting to note that the aberrant phenotypes of *CCRK*-KO cells were not rescued by the exogenous expression of a kinase-dead CCRK mutant or a mutant lacking a short C-terminal region responsible for BROMI binding (Noguchi *et al.*, 2021).

In this study, we first analyzed the potential interactions of CCRK and BROMI with CFAP20 (also known as FAP20, BUG22, and GTL3), as two independent interactome studies suggested that CCRK and BROMI interact directly or indirectly with CFAP20 (Boldt *et al.*, 2016; Huttlin *et al.*, 2017), but the potential interactions have not been characterized in detail to date. We then established *BROMI*-KO cells and compared their phenotypes with those of *CCRK*-KO and *ICK*-KO cells and also analyzed the phenotypes of *BROMI*-KO cells expressing various BROMI mutants. While this study was underway, a FAM149B1-like protein in *C. elegans* was reported to regulate cilia homeostasis via acting upstream of orthologues of CCRK and ICK (Maurya and Sengupta, 2021), although *C. elegans* lacks a BROMI orthologue. Therefore we also investigated how FAM149B1/JBTS36 participates in the regulation of the functions of BROMI and CCRK.

RESULTS

Interaction of CFAP20 with BROMI–CCRK

We recently showed that CCRK/CDK20 interacts with both the N- and the C-terminal regions of BROMI/TBC1D32, and that CCRK regulates the turnaround event of the IFT machinery at the ciliary tip together with BROMI, and probably by phosphorylating ICK/CILK1 (Noguchi *et al.*, 2021). In this study, we first analyzed the potential interactions of BROMI and CCRK with CFAP20/FAP20/BUG22/GTL3 (see Figure 1A) for the following reasons: 1) two independent interactome studies suggested direct or indirect interactions of CCRK and BROMI with CFAP20 (Boldt *et al.*, 2016; Huttlin *et al.*, 2017); 2) CFAP20 is a highly conserved protein, with 89% amino acid identity even between humans and *Chlamydomonas reinhardtii* (Supplemental Figure S1A) (Laligné *et al.*, 2010); 3) CFAP20 was

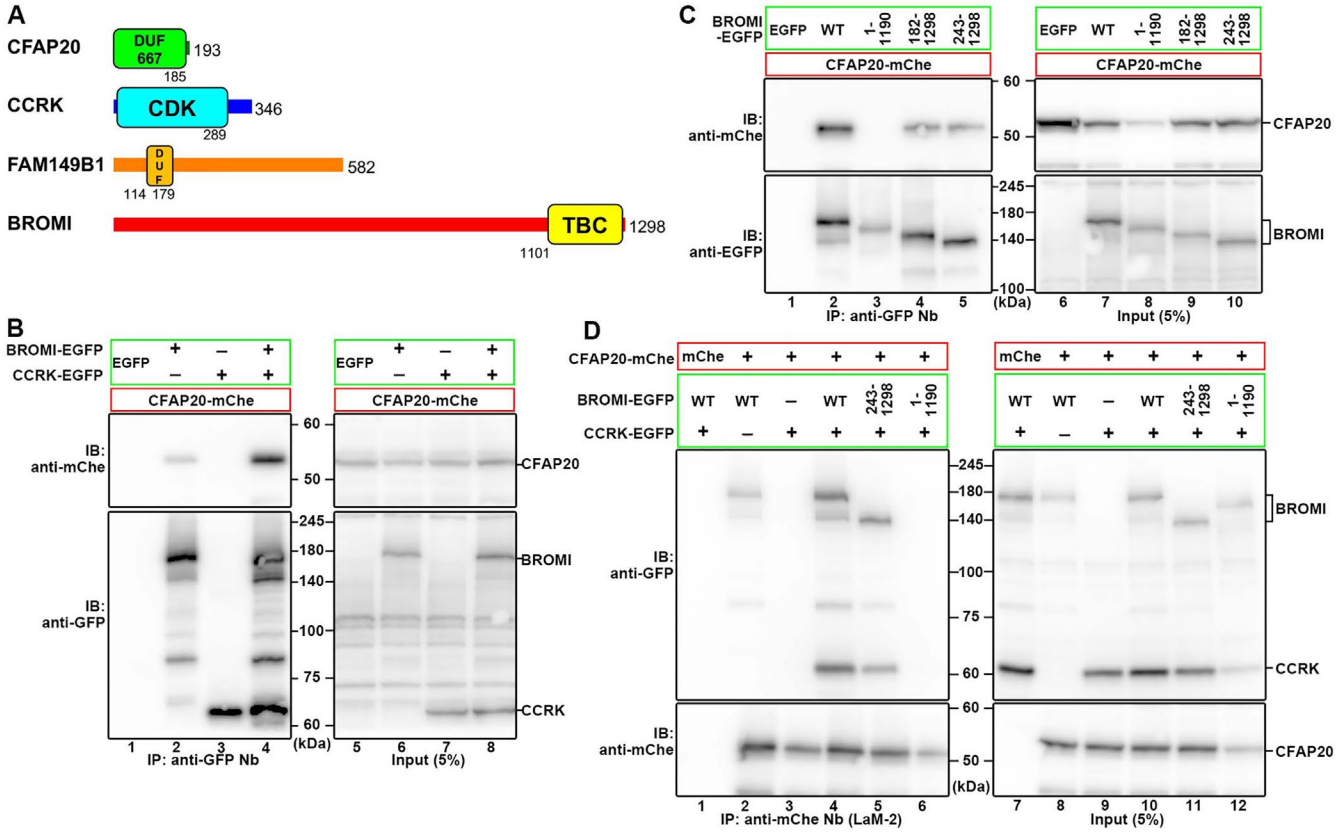

FIGURE 1: Interaction of BROMI with CFAP20 and CCRK. (A) Schematic representation of the domain organizations of CFAP20, CCRK, FAM149B1, and BROMI. DUF in FAM149B1, DUF3719. (B) Direct interaction of CFAP20 with BROMI but not with CCRK. Lysates of HEK293T cells coexpressing CFAP20-mChe and EGFP-fused BROMI or CCRK, or both, were immunoprecipitated with GST-tagged anti-GFP Nb prebound to glutathione–Sepharose 4B beads followed by SDS–PAGE and immunoblotting analysis using an anti-mChe or anti-GFP antibody. (C) BROMI interacts with CFAP20 via its C-terminal region. Lysates of cells coexpressing EGFP-fused BROMI constructs as indicated and CFAP20-mChe were analyzed as described in (B). (D) Lysates of cells coexpressing CFAP20-mChe, CCRK-EGFP, and EGFP-fused BROMI constructs as indicated were immunoprecipitated with GST-tagged anti-mChe Nb (LaM-2 version) prebound to glutathione–Sepharose 4B beads, followed by SDS–PAGE and immunoblotting analysis using an anti-GFP or anti-mChe antibody.

identified by proteome analysis of mammalian cilia (Ishikawa *et al.*, 2012), and FAP20 is a component of the inner junction complex that bridges protofilaments of A- and B-tubules of doublet microtubules in *Chlamydomonas* and *Tetrahymena* (Yanagisawa *et al.*, 2014; Ma *et al.*, 2019; Khalifa *et al.*, 2020). We confirmed that EGFP-fused CFAP20 is evenly distributed within cilia when expressed in hTERT-RPE1 cells (Supplemental Figure S1B). 4) FAP20/BUG22 was reported to be required for ciliary stroke in *Paramecium*, beating of *Chlamydomonas* flagella, and *Drosophila* sperm flagella integrity (Laligné *et al.*, 2010; Maia *et al.*, 2014; Meng *et al.*, 2014; Yanagisawa *et al.*, 2014). 5) Morpholino-mediated knockdown of CFAP20 in zebrafish caused ciliary defect phenotypes, such as a curved body axis and defective heart-looping orientation (Yanagisawa *et al.*, 2014).

When expression vectors for BROMI-EGFP and CFAP20-mCherry (mChe) were coexpressed in HEK293T cells and the lysates prepared from the transfected cells were subjected to immunoprecipitation with glutathione *S*-transferase (GST)-fused anti-green fluorescent protein (GFP) nanobody (Nb) prebound to glutathione–Sepharose beads, BROMI-EGFP coprecipitated CFAP20-mChe (Figure 1B, lane 2). However, coexpression of CCRK-EGFP with BROMI-EGFP caused a substantial increase in the amount of coprecipitated CFAP20-mChe (Figure 1B, compare lane 4 with lane 2; see also Figure 1D, lanes 2 and 4). On the other hand, CFAP20-mChe was not coprecipitated with CCRK-EGFP alone (Figure 1B, lane 3). Thus CFAP20 efficiently interacts with the BROMI-CCRK complex, although it can also bind to BROMI alone.

In a previous study, we showed that BROMI (1298 amino acid protein in humans; Figure 1A) requires both its N-terminal and C-terminal regions to interact with CCRK (Noguchi *et al.*, 2021). We then analyzed which region(s) of BROMI is required for its interaction with CFAP20 (Figure 1C). Truncation of the C-terminal 108 amino acids abolished the interaction of BROMI with CFAP20 (lane 3) as well as with CCRK, as described previously (Noguchi *et al.*, 2021), although the resulting BROMI(1–1190) construct was unstable (lane 8) when expressed in HEK293T cells, as described previously (Noguchi *et al.*, 2021). Truncation of the N-terminal 242 amino acids only slightly reduced the interaction of BROMI with CFAP20 (lane 5) as with CCRK, as described previously (Noguchi *et al.*, 2021). Even in the presence of coexpressed CCRK, the BROMI(1–1,190) construct lacked the ability to interact with CFAP20 (Figure 1D, lane 6), whereas the N-terminal 242 amino acid truncation marginally affected the interaction of BROMI with CFAP20 (Figure 1D, lane 5). Thus the C-terminal region of BROMI encompassing the TBC

domain is required for its interaction with CCRK and CFAP20, and its N-terminal region contributes to its interaction with CCRK and probably makes a minor contribution to its interaction with CFAP20.

BROMI-KO cells phenocopy CCRK-KO and ICK-KO cells

We then attempted to establish *BROMI*-KO and *CFAP20*-KO cells from hTERT-RPE1 cells using the CRISPR/Cas9 system. However, we were unable to obtain *CFAP20*-KO cells probably because CFAP20 is essential for cell survival (Blomen *et al.*, 2015; Wang *et al.*, 2015). When CFAP20-EGFP was stably expressed in RPE1 cells, it was evenly distributed within cilia (Supplemental Figure S1B), consistent with the role of CFAP20 as a component of the inner junction complex of axonemal microtubules (Yanagisawa *et al.*, 2014; Ma *et al.*, 2019; Khalifa *et al.*, 2020). Intriguingly, CFAP20-EGFP signals were reproducibly detected at the daughter centriole (Supplemental Figure S1, B–E), suggesting that CFAP20 is also a component of centriolar triplet microtubules. It is also interesting to note that CFAP20-EGFP signals were reproducibly detected within the nucleus (Supplemental Figure S1, B–E). This observation may be implicated by the fact that interactome studies detected interactions of CFAP20 with FOXJ1 and RFX3, which are master regulatory transcription factors of ciliogenesis (Li *et al.*, 2015; Boldt *et al.*, 2016).

On the other hand, we successfully obtained cell lines with mutations in both alleles of the *BROMI* gene (Supplemental Figure S2, A and B). When cells were serum-deprived for 24 h to induce ciliogenesis and then immunostained for ARL13B and acetylated α-tubulin (Ac-tubulin) as markers of the ciliary membrane and axoneme, respectively, the measured ciliary length was significantly longer in *BROMI*-KO cells than in control RPE1 cells, as was observed for *CCRK*-KO and *ICK*-KO cells (Figure 2, A–D; see also Figure 2M). Despite its direct interaction with BROMI, the localization of CFAP20 in the axoneme and daughter centriole was unaltered in *BROMI*-KO cells as well as in *CCRK*-KO and *ICK*-KO cells (Supplemental Figure S1, B–E).

We also compared the localizations of IFT88 (an IFT-B subunit) and IFT140 (an IFT-A subunit) between control cells and *BROMI*-KO, *CCRK*-KO, and *ICK*-KO cells. In control RPE1 cells, IFT88 was found mainly at the ciliary base and a small proportion at the tip (Figure 2E). By contrast, a substantial proportion of IFT88 was found at the ciliary tip in *BROMI*-KO cells (Figure 2F) as well as in *CCRK*-KO and *ICK*-KO cells (Figure 2, G and H; see also Figure 2N), as described previously (Noguchi *et al.*, 2021). Similar results were obtained for the localization of IFT140 (Figure 2, I–L, O). Furthermore, exogenously expressed EGFP-fused KAP3 (also known as KIFAP3), a subunit of the anterograde motor kinesin-II (Figure 3, A–D, I), and DYNC2LI1, a subunit of the retrograde motor dynein-2 (Figure 3, E–H, J), were also significantly enriched at the ciliary tip of *BROMI*-KO cells as well as *CCRK*-KO and *ICK*-KO cells compared with control RPE1 cells. These observations, therefore, suggest that kinesin-to-dynein motor switching or the initiation of retrograde trafficking after the switching is at least partially impaired in the absence of BROMI, CCRK, or ICK.

We also compared the localization of exogenously expressed mChe-ICK. Our previous study showed that in *CCRK*-KO cells, ICK is accumulated at the ciliary tip (Noguchi *et al.*, 2021), probably because in the absence of CCRK, ICK does not undergo phosphorylation at the TXY motif and thereby cannot participate in the turnaround event of the IFT machinery; ICK itself is a cargo of the IFT machinery (Nakamura *et al.*, 2020). As shown in Figure 2R, mChe-ICK was enriched at the ciliary tip in *CCRK*-KO cells compared with control RPE1 cells (Figure 2P). In *BROMI*-KO cells, mChe-ICK was also enriched at the tip (Figure 2Q), suggesting that in the absence of BROMI, ICK is not functional after its transportation to the tip, as in the absence of CCRK.

Our previous studies showed that proteins accumulated at the tips of *CCRK*-KO and *ICK*-KO cilia are often eliminated via ECVs (Nakamura *et al.*, 2020; Noguchi *et al.*, 2021), and we found that this was also the case for *BROMI*-KO cells. As shown in Figure 2, S and T (see also Supplemental Videos S1 and S2), the release of ARL13B-positive ECVs from the tip was observed in *BROMI*-KO cells. These observations altogether indicate that the change in the direction of the IFT machinery at the ciliary tip is impaired in *BROMI*-KO cells as well as in *CCRK*-KO and *ICK*-KO cells.

Next, we compared the ciliary localizations of GPR161 and Smoothened (SMO) between *BROMI*-KO and control, *CCRK*-KO, or *ICK*-KO cells. GPR161 and SMO are class A and class F GPCRs, respectively, and regulate Hh signaling in negative and positive manners, respectively (Anvarian *et al.*, 2019; Kopinke *et al.*, 2021). In control RPE1 cells, GPR161 is present on the ciliary membrane, whereas SMO is excluded from cilia in the basal state (Figure 4, A and I). When the Hh pathway was stimulated by treatment of cells with Smoothened Agonist (SAG), GPR161 exited and SMO entered cilia (Figure 4, E and M). In *BROMI*-KO cells, the basal ciliary levels of GPR161 and SMO were significantly higher than those in control RPE1 cells (Figure 4, B and J); in particular, SMO was occasionally found enriched at the tip (Figure 4J). In the presence of SAG, the GPR161 level within cilia was sustained, and the SMO level was further increased (Figure 4, F and N; see also Figure 4, Q and R). Essentially the same trends in ciliary GPR161 and SMO levels in the absence and presence of SAG treatment were observed in *CCRK*-KO and *ICK*-KO cells (Figure 4, C, D, G, H, K, L, O–R). Taking into account the facts that ICK is phosphorylated by CCRK (Fu *et al.*, 2005, 2006), and that CCRK and BROMI form a complex (Noguchi *et al.*, 2021), the phenotypic similarities among *BROMI*-KO, *CCRK*-KO, and *ICK*-KO cells are consistent with the notion that CCRK regulates ICK function together with BROMI.

BROMI requires its interactions with CCRK and probably with CFAP20 for its function

The length of cilia of *BROMI*-KO cells was restored to that of control cells by the stable expression of EGFP-fused BROMI(wild type [WT]) but not EGFP alone (Figure 5, A–C; see also Figure 5P). Similarly, the accumulation of IFT88 and IFT140 at the ciliary tip was also rescued by the expression of BROMI(WT)-EGFP but not EGFP (Figure 5, F–H and K–M; see also Figure 5, Q and R). By contrast, BROMI mutants lacking the N-terminal or C-terminal region did not significantly rescue the ciliary defects. *BROMI*-KO cells expressing EGFP-fused BROMI(243–1298) or BROMI(1–1190) had significantly longer cilia (Figure 5, D and E) and significantly more intense staining for IFT88 (Figure 5, I and J) and IFT140 (Figure 5, N and O) at the tip than cells expressing BROMI(WT)-EGFP (see also Figure 5, P–R). Although we could not detect the clear localization of any of the expressed BROMI constructs within cilia or around the ciliary base, low levels of expression of the EGFP-fused BROMI constructs were confirmed by immunoblotting analysis of lysates of *BROMI*-KO cells expressing the EGFP-fused BROMI constructs using anti-GFP antibody (Figure 5S). Taken together with a previous study showing that BROMI(1–1190) lacks CCRK-binding ability, and that BROMI(243–1298) has reduced CCRK-binding ability (Noguchi *et al.*, 2021) as well as the data of Figure 1 showing the lack of CFAP20 binding to BROMI(1–1190) but not that to BROMI(243–1298), the interactions of BROMI with CCRK and probably with CFAP20 are expected to be required for its function.

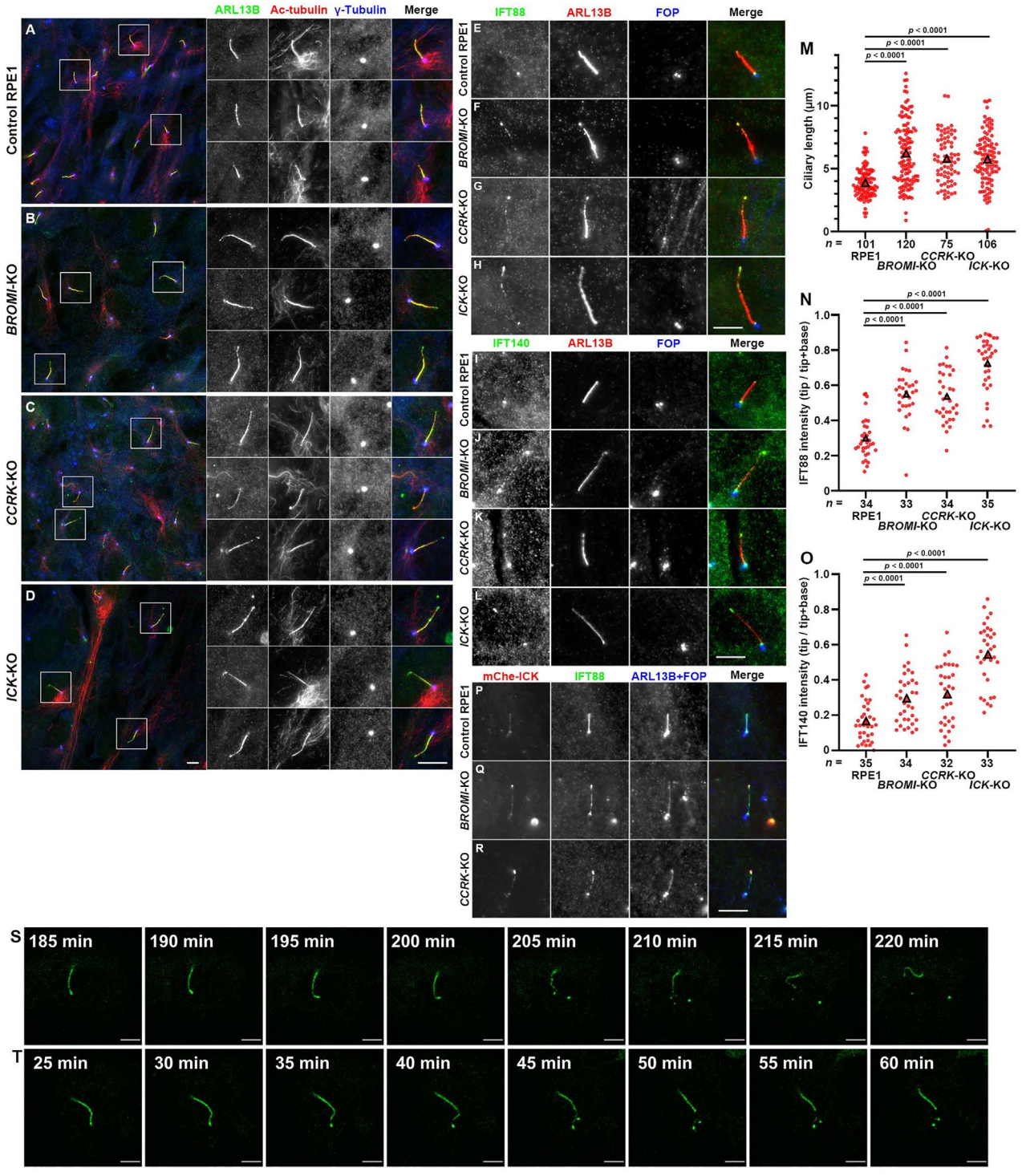

FIGURE 2: Cilia elongation and accumulation of IFT components at the ciliary tip in *BROMI*-KO cells. (A–L) Control RPE1 cells (A, E, I), the *BROMI*-KO cell line #BROMI-2-17 (B, F, J), the *CCRK*-KO cell line #CCRK-2-4 (C, G, K), and the *ICK*-KO cell line #ICK-4-6 (D, H, L) were cultured under serum-starved conditions for 24 h to induce ciliogenesis and triple immunostained for ARL13B, acetylated α-tubulin, and γ-tubulin (A–D); IFT88, ARL13B, and FOP (recently renamed as CEP43) (E–H); or IFT140, ARL13B, and FOP (I–L). Scale bars, 5 μm. (M) Ciliary lengths of the cells in (A)–(D) were measured and expressed as scatter plots. (N, O) Relative staining intensities of IFT88 and IFT140 at the ciliary tips and base in the cells shown in (E)–(H) and (I)–(L), respectively, were estimated, and the intensity ratios of tip/(tip+base) were expressed as scatter plots. The total number of cells analyzed (*n*) are indicated. The triangles indicate the means. Statistical significances were calculated using one-way ANOVA followed by the Dunnett's multiple comparison test. (P–R) Control RPE1 cells (P), *BROMI*-KO cells (Q), and *CCRK*-KO cells (R) stably expressing mChe-ICK were serum-deprived for 24 h and immunostained for IFT88 and ARL13B+FOP. Scale bar, 5 μm. (S, T) The release of ECVs from the ciliary tips of the *BROMI*-KO cells stably expressing ARL13B(ΔGD)-EGFP. Time-lapse images of Supplemental Videos S1 and S2 are shown. Scale bars, 5 μm.

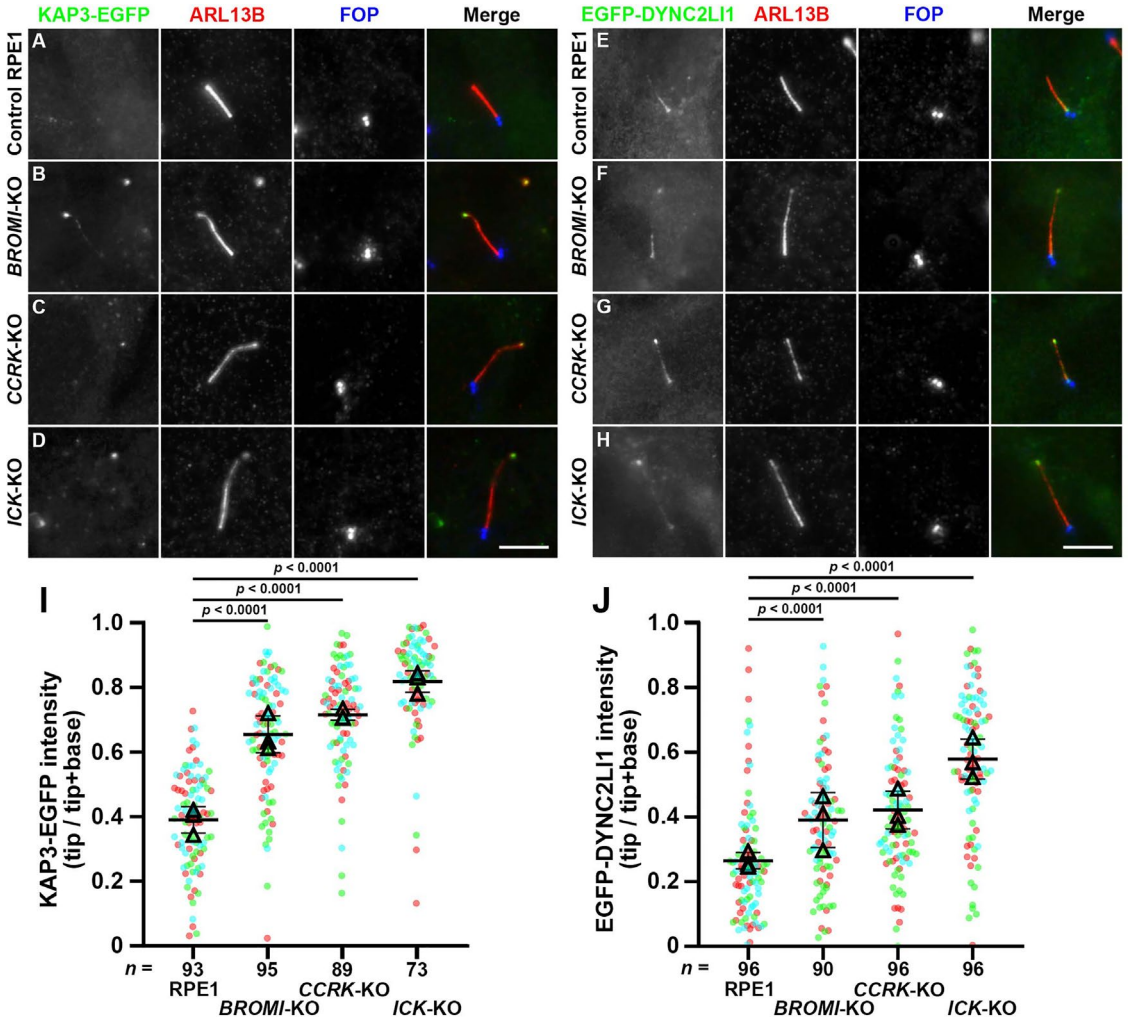

FIGURE 3: Accumulation of kinesin-II and dynein-2 at the ciliary tips of *BROMI*-KO cells. (A–H) Control RPE1 cells (A, E), *BROMI*-KO cells (B, F), *CCRK*-KO cells (C, G), and *ICK*-KO cells (D, H) stably expressing KAP3-EGFP (A–D) or EGFP-DYNC2LI1 (E–H) were serum-deprived for 24 h and double immunostained for ARL13B and FOP. Scale bars, 5 μm. (I, J) The intensities of KAP3-EGFP (I) and EGFP-DYNC2LI1 (J) signals in the tip and base regions in individual cells were measured, and their intensity ratios, i.e., tip/(tip+base), were represented as scatter plots. The total number of cells analyzed (*n*) are indicated. Differently colored dots represent three independent experiments, and triangles are the means of individual experiments. Horizontal lines and error bars are means and SD, respectively, of the three experiments. Statistical significances were calculated using one-way ANOVA followed by the Dunnett's multiple comparison test.

Interactions of FAM149B1 with BROMI–CFAP20 and with CCRK

While this study was in progress, a *C. elegans* study reported that the FAM149B1-like protein XBX-4 may act via a pathway involving CCRK and ICK orthologues (DYF-18 and DYF-5) to regulate cilia homeostasis (Maurya and Sengupta, 2021), although there is no direct orthologue of BROMI in the *C. elegans* genome. On the other hand, previous case studies reported that homozygous mutations in *FAM149B1* cause JBTS-associated diseases in humans, resulting in abnormal ciliary phenotypes such as tip accumulation of IFT-B and dysregulation of the Hh signaling (Shaheen *et al.*, 2019; Siegert *et al.*, 2021), and an interactome study suggested direct or indirect interactions of FAM149B1 with BROMI and CFAP20 (Huttlin *et al.*, 2017). However, as shown in Figure 6A, coimmunoprecipitation analysis showed that the interaction of BROMI with FAM149B1 was relatively weak (lane 3). We then analyzed the FAM149B1–BROMI interaction in the presence of CFAP20, and found that the interaction of FAM149B1 with BROMI was substantially enhanced in the presence of coexpressed CFAP20 (compare lane 5 with lane 3), although FAM149B1 did not demonstrate a direct interaction with CFAP20 alone (lane 4).

FAM149B1 has a domain of unknown function 3719 (DUF3719) in its N-terminal region (Figure 1A), and homozygous mutations in this domain resulting in premature termination (p.Gln118Hisfs*20, p.Lys119Ilefs*18, and p.Gln147*) were found to cause JBTS-associated diseases (Shaheen *et al.*, 2019; Siegert *et al.*, 2021). When the FAM149B1 protein was divided into the DUF3719-containing region, FAM149B1(1–179), and the remaining region, FAM149B1(180–582) (see Figure 1A), the latter retained the ability, although reduced, to interact with BROMI–CFAP20 (Figure 6B; compare lanes 3 and 4 with lane 2), indicating that the non-DUF3719 region of FAM149B1 mainly contributes to its interaction with BROMI–CFAP20. This was somewhat unexpected, as the non-DUF3719 region is not conserved between *C. elegans* and vertebrates (Maurya and Sengupta, 2021),

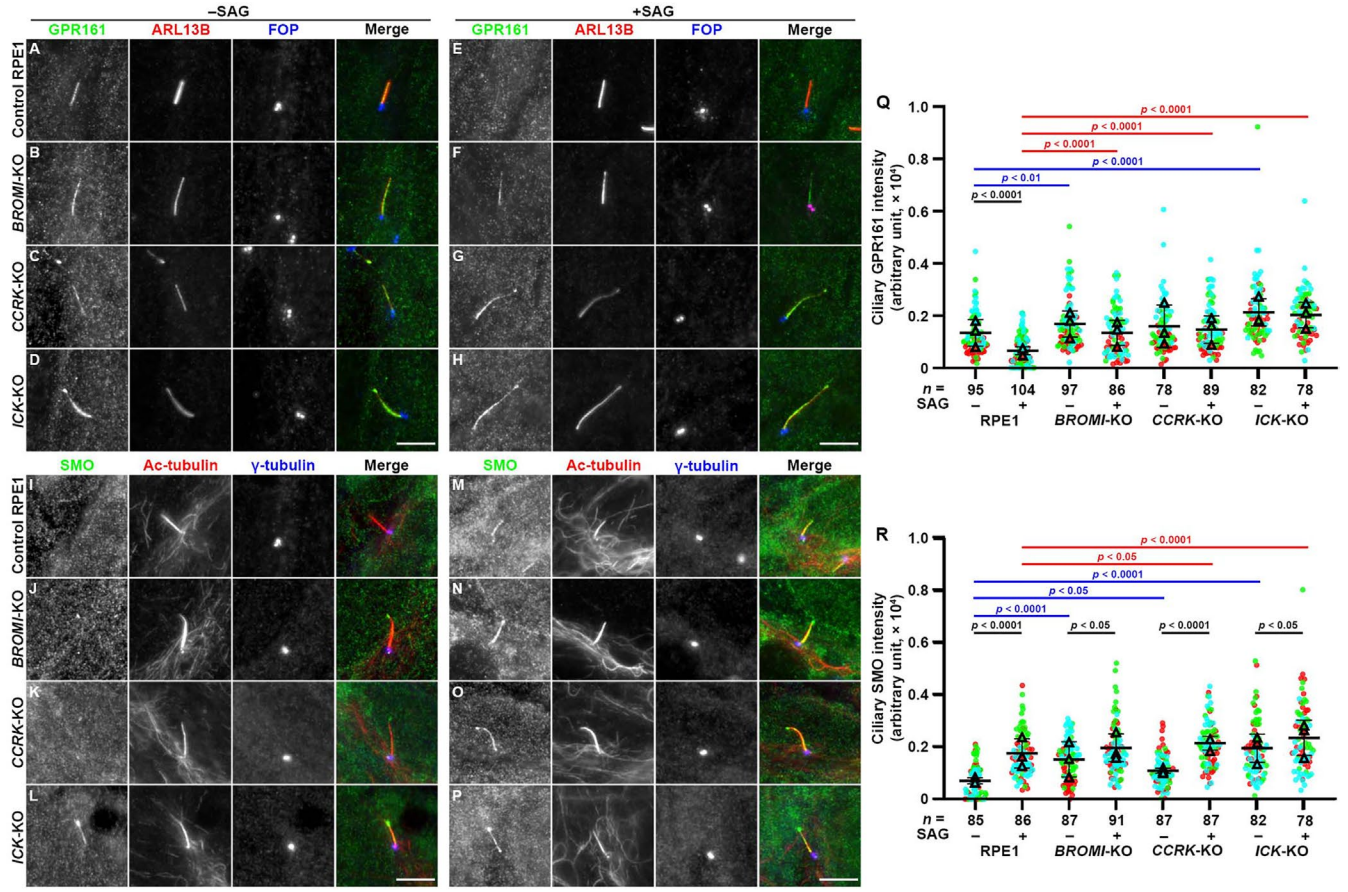

FIGURE 4: Accumulation of GPR161 and SMO within cilia of *BROMI*-KO cells. (A–P) Control RPE1 cells (A, E, I, M), *BROMI*-KO cells (B, F, J, N), *CCRK*-KO cells (C, G, K, O), and *ICK*-KO cells (D, H, L, P) were serum-starved for 24 h and further incubated for 24 h without (–SAG; A–D, I–L) or with (+SAG; E–H, M–P) 200 nM SAG. The cells were triple immunostained for GPR161 (A–H), ARL13B, and FOP or for SMO (I–P), Ac-tubulin, and γ-tubulin. Scale bars, 5 μm. (Q, R) The relative ciliary staining intensities of GPR161 and SMO shown in (A–H) and (I–P), respectively, were estimated and expressed as scatter plots. The total number of cells analyzed (*n*) is indicated. Differently colored dots represent three independent experiments, and triangles are means of individual experiments. Horizontal lines and error bars are means and SDs, respectively, of the three experiments. Statistical significances among multiple cell lines were calculated using one-way ANOVA followed by the Dunnett's multiple comparison test.

although there is no BROMI orthologue in *C. elegans*. Although the C-terminal nonconserved region of FAM149B1 is predicted to be intrinsically disordered (see *Discussion*), it did not nonspecifically interact with EGFP alone (Supplemental Figure S3).

We then analyzed whether CCRK can interact indirectly with FAM149B1 via BROMI–CFAP20. To this end, TagBFP (tBFP)-tagged CCRK was coexpressed with FAM149B1-mChe in the presence or absence of coexpressed BROMI-EGFP and/or CFAP20-EGFP in HEK293T cells, and lysates from the cells were subjected to immunoprecipitation with GST-fused anti-mChe Nb (the LaM-2 version) prebound to glutathione Sepharose 4B beads. As shown in Figure 6C, CCRK substantially coprecipitated with FAM149B1 in the presence of BROMI+CFAP20 (lane 5) and moderately in the presence of BROMI alone (lane 3). The amount of BROMI+CFAP20 coprecipitated with FAM149B1 was greater in the presence of coexpressed CCRK than in its absence (compare lane 5 with lane 6), suggesting that the interaction of FAM149B1 with BROMI–CFAP20 is enhanced in the presence of CCRK. Intriguingly, a low but substantial amount of CCRK was coprecipitated with FAM149B1 even in the absence of coexpressed BROMI+CFAP20 (lane 2) or in the presence of coexpressed CFAP20 alone (lane 4), suggesting a direct interaction of FAM149B1 with CCRK. This was also unexpected, as to our knowledge, no interactome studies to date have suggested an interaction between FAM149B1 and CCRK.

We then analyzed whether the DUF3719 region or the non-DUF3719 region of FAM149B1 interacts directly with CCRK under the prediction that the conserved DUF3719 region is important for this interaction. As shown in Figure 6D, however, the non-DUF3719 region (residues 180–582) was found to interact with CCRK (lane 4). Thus the non-DUF3719 region of FAM149B1 is mainly responsible for its interactions with both CCRK and BROMI (Figure 6E). In the AlphaFold Protein Structure Database (Tunyasuvunakool *et al.*, 2021), the non-DUF3719 region is predicted to be unstructured, suggesting that this region has the potential to interact with a variety of proteins as "an intrinsically disordered region."

Ciliary defects of FAM149B1-KO cells resemble those of BROMI-KO, CCRK-KO, and ICK-KO cells

We next established *FAM149B1*-KO cells from hTERT-RPE1 cells (Supplemental Figure S2, C and D) and analyzed their phenotypes. *FAM149B1*-KO cells had longer cilia and demonstrated substantial accumulation of IFT88 at the ciliary tip compared with control RPE1

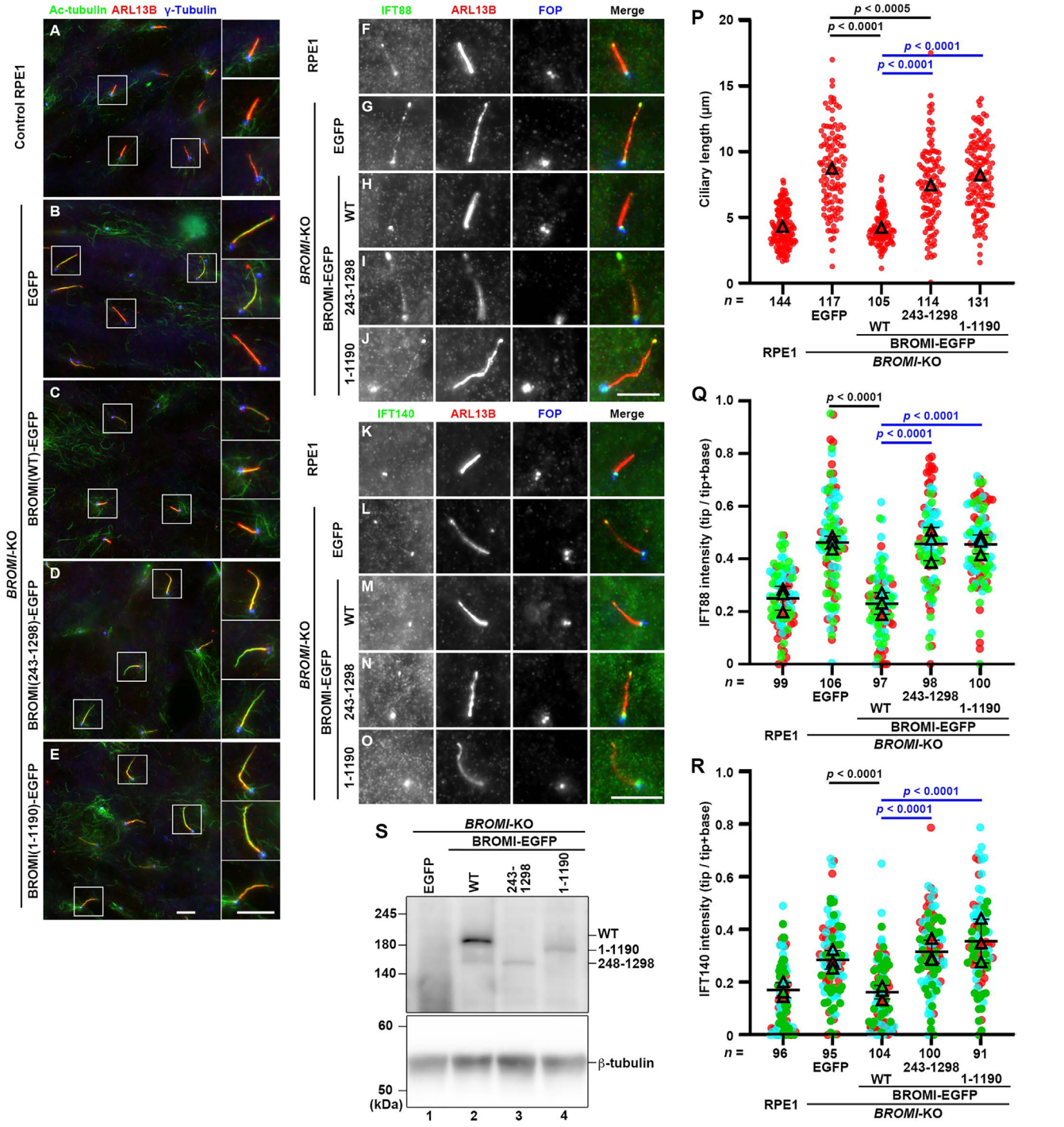

FIGURE 5: BROMI requires its interaction with CCRK and probably with CFAP20 for its functions. (A–O) Control RPE1 cells (A, F, K), or *BROMI*-KO cells stably expressing EGFP (B, G, L), or EGFP-fused BROMI(WT) (C, H, M), BROMI(243–1,298) (D, I, N), or BROMI(1–1,190) (E, J, O) were serum-deprived for 24 h and triply immunostained for Ac-tubulin, ARL13B, and γ-tubulin (A–E); IFT88, ARL13B, and FOP (F–J); or IFT140, ARL13B, and FOP (K–O). Scale bars, 5 μm. Note that the EGFP epifluorescence was quenched when the cells were fixed with methanol. (P) Ciliary lengths of the cells in (A)–(E) were measured and expressed as scatter plots. The total number of cells analyzed (*n*) are indicated. The triangles indicate the means. (Q, R) Relative staining intensities of IFT88 and IFT140 at the ciliary tips and base in the cells shown in (F)–(J) and (K)–(O), respectively, were estimated, and the intensity ratios of tip/(tip+base) were expressed as scatter plots. Differently colored dots represent three independent experiments, and triangles are means of individual experiments. Horizontal lines and error bars are means and SD, respectively, of the three experiments. Statistical significances were calculated using one-way ANOVA followed by the Dunnett's multiple comparison test. (S) Lysates prepared from *BROMI*-KO cells stably expressing EGFP (lane 1) or EGFP-fused BROMI(WT) (lane 2), BROMI(243–1,298) (lane 3), or BROMI(1–1,190) (lane 4) were processed for immunoblotting analysis using an anti-GFP or anti-β-tubulin antibody.

FIGURE 6: Interactions of FAM149B1 with BROMI and CCRK. (A) Direct interaction of FAM149B1 with BROMI but not with CFAP20. Lysates of HEK293T cells coexpressing FAM149B1-mChe and EGFP-fused BROMI or CFAP20, or both, were immunoprecipitated with GST-tagged anti-mChe Nb (LaM-2 version) prebound to glutathione–Sepharose 4B beads, followed by SDS–PAGE and immunoblotting analysis using an anti-EGFP or anti-mChe antibody. (B) FAM149B1 interacts with BROMI via its non-DUF3719 region. Lysates of cells coexpressing mChe-fused FAM149B1 constructs, as indicated, and EGFP-fused BROMI and CFAP20 were analyzed as described in (A). (C) Indirect and direct interactions of FAM149B1 with CCRK. Lysates of cells coexpressing mChe-fused FAM149B1 constructs as indicated, and CCRK-tBFP, and combinations of BROMI-EGFP and CFAP20-EGFP as indicated were immunoprecipitated with GST-tagged anti-mChe Nb (LaM-2) followed by SDS–PAGE and then subjected to immunoblotting analysis using an anti-tRFP antibody that recognizes tBFP, an anti-GFP antibody, or an anti-mChe antibody. (D) FAM149B1 interacts with CCRK via its non-DUF3719 region. Lysates of cells coexpressing mChe-fused FAM149B1 constructs as indicated and CCRK-EGFP were analyzed as described in (A). (E) A model of the interactions among BROMI, CCRK, FAM149B1, and CFAP20 predicted from this study. The coloring of the individual proteins is the same as shown in Figure 1A.

cells (Figure 7, A and B; see also Figure 7, F and G); this is in line with the observation of fibroblasts from a patient with JBTS-like symptoms with the homozygous FAM149B1 mutation (Shaheen *et al.*, 2019). Stable expression of FAM149B1(WT)-EGFP in *FAM149B1*-KO cells restored normal ciliary length and eliminated abnormal IFT88 accumulation at the tip (Figure 7C; see also Figure 7, F and G). As in *BROMI*-KO and *CCRK*-KO cells (Figure 2Q, R), stably expressed mChe-ICK was substantially enriched at the ciliary tip of *FAM149B1*-KO cells compared with control RPE1 cells (Figure 7, H and I). CFAP20 localization to the ciliary axoneme and daughter centriole was unaltered in *FAM149B1*-KO cells (Supplemental Figure S1F, G), consistent with the observation in the *C. elegans*

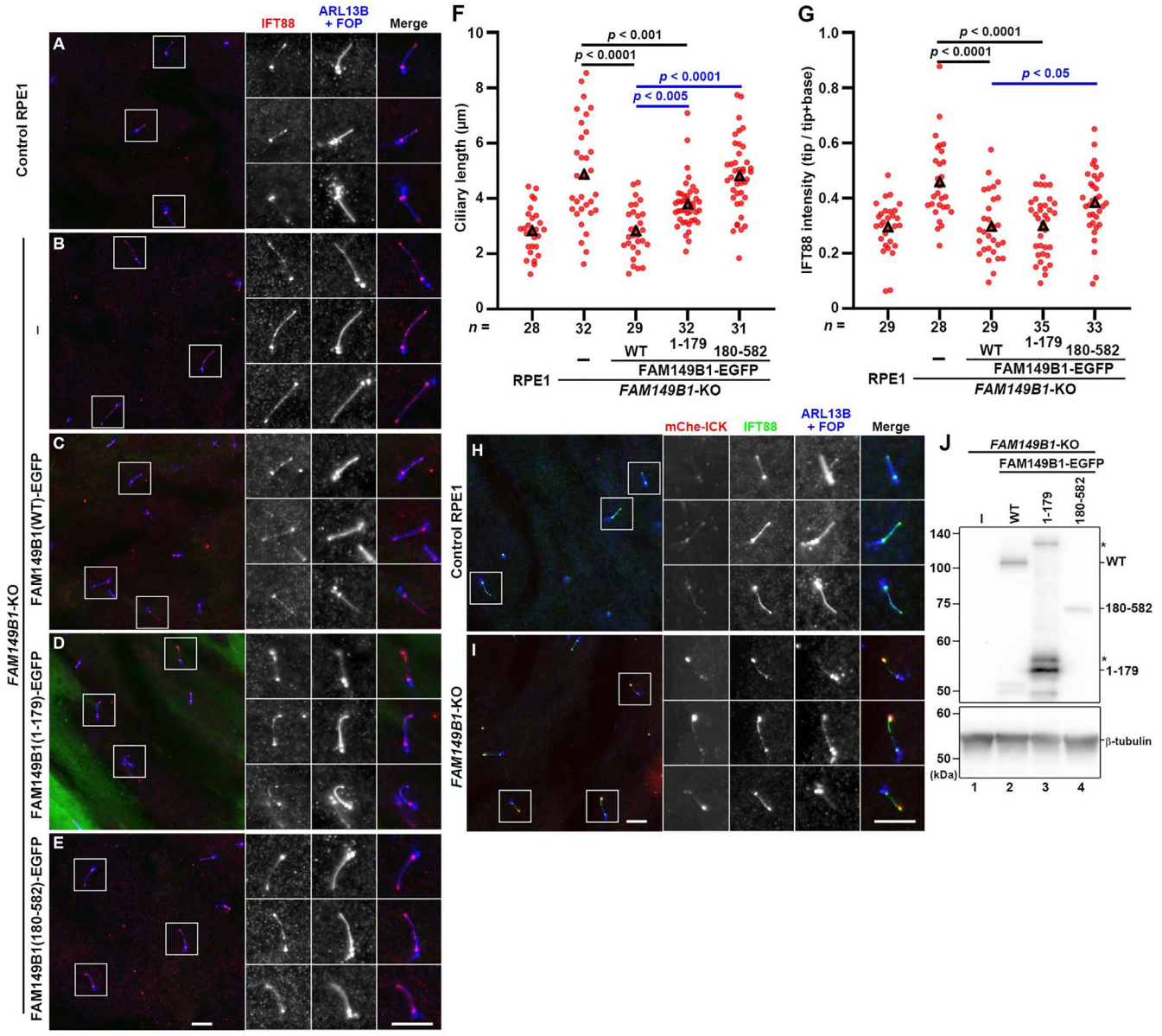

FIGURE 7: *FAM149B1*-KO cells phenocopy *BROMI*-KO, *CCRK*-KO, and *ICK*-KO cells. (A–E) Control RPE1 cells (A) and *FAM149B1*-KO cells (B) and those stably expressing EGFP-fused FAM149B1(WT), FAM149B1(1–179), or FAM149B1(180–582) were cultured under serum-starved conditions for 24 h and immunostained for IFT88 and ARL13B+FOP. Scale bars, 5 μm. (F) Ciliary lengths of the cells shown in (A)–(E) were measured and expressed as scatter plots. (G) Relative staining intensities of IFT88 at the ciliary tip and base in the cells shown in (A)–(E) were estimated, and the intensity ratio of tip/(tip+base) was expressed as scatter plots. The total number of cells analyzed (*n*) are indicated. The triangles indicate the means. Statistical significances were calculated using one-way ANOVA followed by the Dunnett's multiple comparison test. (H, I) Control RPE1 cells (H) and *FAM149B1*-KO cells (I) stably expressing mChe-ICK were serum-deprived for 24 h and immunostained for IFT88 and ARL13B+FOP. Scale bar, 5 μm. (J) Lysates prepared from *FAM149B1*-KO cells (lane 1) and those stably expressing EGFP-fused FAM149B1(WT) (lane 2), FAM149B1(1–179) (lane 3), or FAM149B1(180–582) (lane 4) were processed for immunoblotting analysis using an anti-GFP or anti-β-tubulin antibody. Asterisks indicate the positions of nonspecific bands of unknown origin.

xbx-4 mutant (Maurya and Sengupta, 2021). Thus *FAM149B1*-KO cells phenocopy *BROMI*-KO, *CCRK*-KO, and *ICK*-KO cells with respect to their ciliary defects (Figure 2) and are likely to be impaired with respect to the turnaround process at the tip.

When the N-terminal [FAM149B1(1–179)] or C-terminal [FAM149B1(180–582)] construct was expressed in *FAM149B1*-KO cells, cilia did not recover to the normal length as in the case of FAM149B1(WT) expression (Figure 7, C–E; see also Figure 7F). However, somewhat unexpected was that the expression of FAM149B1(1–179) in *FAM149B1*-KO cells significantly rescued the defect in IFT88 accumulation at the tip similarly to the FAM149B1(WT) expression (Figure 7G). Immunoblot analysis of cell lysates confirmed the expression of the FAM149B1 constructs (Figure 7J). Although we do not know the exact reason for this observation, it suggests that the conserved DUF3719 region plays some role in ciliary protein trafficking independently of CCRK and BROMI.

DISCUSSION

Mutations in *BROMI*, *CCRK*, *ICK*, *and FAM149B1* in humans are known to cause ciliopathies, and those in mice cause ciliopathy-like phenotypes with impaired Hh signaling (Lahiry *et al.*, 2009; Adly *et al.*, 2014; Oud *et al.*, 2016; Taylor *et al.*, 2016; Snouffer *et al.*, 2017; Shaheen *et al.*, 2019; Alsahan and Alkuraya, 2020; Hietamäki *et al.*, 2020; Siegert *et al.*, 2021). In previous studies, we showed that ICK undergoes IFT-mediated trafficking to the ciliary tip where it regulates the IFT turnaround event in a manner dependent on its phosphorylation cycle involving CCRK (Nakamura *et al.*, 2020; Noguchi *et al.*, 2021).

In this study, we showed that BROMI interacts not only with CCRK but also with CFAP20, which is a conserved axonemal protein, and with FAM149B1, a protein in which its mutations cause JBTS-associated diseases. We also found that FAM149B1 interacts directly with CCRK as well as with BROMI. *CCRK*-KO, *BROMI*-KO, and *FAM149B1*-KO cells were found to demonstrate very similar ciliary defects to *ICK*-KO cells, including abnormal cilia elongation and the accumulation of components of the IFT machinery at the ciliary tip. In addition, ICK itself was accumulated at the tip in these KO cells. These observations indicate that interactions of BROMI with CCRK and probably with CFAP20 are crucial for the turnaround process that is controlled by ICK. The data also suggest that FAM149B1 participates in the CCRK–ICK pathway via directly interacting with both BROMI and CCRK. By elucidating the direct interactions among these components and demonstrating the similarity among cells defective in any of these components, the present study, in conjunction with previous studies on ICK and CCRK (Nakamura *et al.*, 2020; Noguchi *et al.*, 2021), expands on the previous studies in *C. elegans* suggesting that orthologues of FAM149B1 (XBX-4), CCRK (DYF-18), and ICK (DYF-5) regulate cilia homeostasis in the same pathway (Yi *et al.*, 2018; Maurya *et al.*, 2019; Maurya and Sengupta, 2021), although *C. elegans* lacks a BROMI orthologue. The direct interaction of FAM149B1 with CCRK suggests that the FAM149B1orthologue can regulate the CCRK orthologue in the absence of a BROMI orthologue. In this context, it is also noteworthy that a CCRK orthologue (LF2) in *Chlamydomonas* forms a complex with LF1 and LF3 (Tam *et al.*, 2007), and *lf1*, *lf2*, *lf3*, and *lf4* mutant strains demonstrate elongated flagella (Asleson and Lefebvre, 1998), although LF1 and LF3 homologues are not present in mammals and *Chlamydomonas* lacks BROMI and FAM149B1 homologues. Thus the core kinases, CCRK and ICK/MAK/MOK, are likely to undergo fine tuning by species-specific modulators.

The common defects found in *ICK*-KO, *CCRK*-KO, *BROMI*-KO, and *FAM149B1*-KO cells are likely to reflect the impaired function of ICK at the ciliary tip. However, we previously showed that CCRK is localized around the base of cilia (Noguchi *et al.*, 2021) but is not detectable within or at the tip of cilia (Ko *et al.*, 2010; Noguchi *et al.*, 2021). In this context, it is of note that *C. elegans* DYF-18 as well as DYF-5 were reported to be in the distal segments of sensory cilia in one study (Yi *et al.*, 2018), whereas in another study both were found in the proximal regions in WT animals (Maurya *et al.*, 2019). On the other hand, consistent with our observations regarding the localization of ICK, DYF-5 was enriched in the distal regions of cilia in *dyf-18* and *xbx-4* mutants (Maurya *et al.*, 2019; Maurya and Sengupta, 2021). In addition, we were unable to show in this study the distinct ciliary localization of BROMI and FAM149B1, although a low level of *C. elegans* XBX-4 was found in the distal region and underwent IFT movement in only a subset of cilia, suggesting that it can be transported via IFT (Maurya and Sengupta, 2021). Furthermore, proteomic analysis of cilia demonstrated that BROMI is a ciliary protein (Ishikawa *et al.*, 2012).

Therefore where and how CCRK phosphorylates/activates ICK in conjunction with BROMI and FAM149B1 are important issues. One possible scenario is that ICK is phosphorylated by CCRK at the base of cilia under the control of BROMI and/or FAM149B1 and is then transported to the ciliary tip via binding to the IFT machinery (Nakamura *et al.*, 2020). As CCRK/CDK20 is a remote member of the CDK family (Malumbres, 2014), BROMI and/or FAM149B1 may play roles as cyclins via directly interacting with CCRK. Given that FAM149B1, but not BROMI, is evolutionarily conserved, and that FAM149B1 can interact directly with CCRK, it is possible that FAM149B1 is the main regulator of CCRK/CDK20 function, similar to cyclins, and that BROMI acts as an adaptor between them to strengthen their interaction (see Figure 6E). In this context, it is an interesting issue whether BROMI and/or FAM149B1 affect the localization of CCRK. However, attempts to determine whether there is a difference in CCRK localization between control cells and *BROMI*-KO or *FAM149B1*-KO cells have so far been unsuccessful because the CCRK-EGFP signals at the ciliary base in control cells are very weak as described previously (Noguchi *et al.*, 2021). Another possibility is that CCRK (as well as BROMI and FAM149B1) can transiently enter cilia and phosphorylate ICK, which in turn regulates the turnaround event at the tip, as a cilia proteome study identified BROMI as a ciliary protein (Ishikawa *et al.*, 2012).

We also showed here that CFAP20 directly interacts with BROMI and enhances the interactions of BROMI with CCRK and FAM149B1, although we were unable to elucidate the physiological relevance of the interactions involving CFAP20, as we could not establish *CFAP20*-KO cells probably owing to its essential role in cell survival (Blomen *et al.*, 2015; Wang *et al.*, 2015). In addition to its role as an integral component of the ciliary axoneme (Yanagisawa *et al.*, 2014; Ma *et al.*, 2019; Khalifa *et al.*, 2020), CFAP20 is also found in the nucleus (Supplemental Figure S1, B–G) and was found to interact with master regulators of ciliogenesis in two independent interactome studies (Li *et al.*, 2015; Boldt *et al.*, 2016). Thus this relatively compact protein may play a variety of roles associated with cilia.

MATERIALS AND METHODS

Request a protocol through *Bio-protocol*.

Plasmids, antibodies, reagents, and cell lines

cDNAs for human CFAP20 (NM_013242.3) and FAM149B1 (NM_173348.2) were obtained from a cDNA library by PCR amplification. Human ICK cDNA was kindly provided by Takahisa Furukawa (Osaka University) (Chaya *et al.*, 2014). Expression vectors for BROMI, CFAP20, FAM149B1, CCRK, and ICK and their deletion and point mutants and vectors for the production of lentiviruses expressing them are listed in Supplemental Table S1. Several of the vectors were constructed in our previous studies (Hamada *et al.*, 2018; Nakamura *et al.*, 2020; Noguchi *et al.*, 2021). Antibodies used in this study are listed in Supplemental Table S2. GST-tagged anti-GFP Nb and anti-mChe Nb (the LaM-2 version) prebound to glutathione–Sepharose 4B beads were prepared as described previously (Katoh *et al.*, 2015; Katoh *et al.*, 2018; Ishida *et al.*, 2021). SAG and Polyethylenimine Max were purchased from Enzo Life Sciences and Polysciences, respectively. HEK293T cells and hTERT-RPE1 cells were obtained from RIKEN BioResource Research Center (Catalogue No. RBC2202) and American Type Culture Collection (Catalogue No. CRL-4000), respectively.

Coimmunoprecipitation analyses

Coimmunoprecipitation analyses were performed based on the procedures described previously for the visible immunoprecipitation

assay using anti-GFP Nb or anti-mChe Nb (LaM-2 version) (Katoh *et al.*, 2015; Nishijima *et al.*, 2017; Ishida *et al.*, 2021). Briefly, HEK293T cells grown on a 6-well plate were cotransfected with expression vectors for EGFP-fused and mChe-fused proteins and those for tBFP-fused proteins, when indicated, using Polyethylenimine Max and cultured for 24 h in high-glucose DMEM (Nacalai Tesque) supplemented with 5% fetal bovine serum (FBS). The transfected cells were then lysed in 250 µl of HMDEKN cell-lysis buffer (10 mM HEPES [pH 7.4], 5 mM $MgSO_4$, 1 mM DTT, 0.5 mM EDTA, 25 mM KCl, and 0.05% NP-40) containing protease inhibitor cocktail (Nacalai Tesque) by incubation for 20 min on ice. The lysates were then centrifuged at 16,100 × *g* for 15 min, and supernatants (200 µl) were transferred to a 0.2-ml 8-tube strip to which GST-tagged anti-GFP Nb or anti-mChe Nb prebound to glutathione–Sepharose 4B beads (approximately 5 µl bed volume of the beads) was added and incubated for 1 h at 4°C with constant rotation of the tube strip. After brief centrifugation at 2,000 × *g* for 10 s, the beads were washed three times with 180 µl of lysis buffer and boiled in SDS–PAGE sample buffer, and the proteins were separated by SDS–PAGE and electroblotted onto a TransBlot Turbo PVDF membrane (Bio-Rad). The membrane was then blocked in 5% skimmed milk and incubated sequentially with primary antibody (anti-GFP, anti-mChe, or anti-tRFP) and peroxidase–conjugated secondary antibody. Protein bands were detected using a Chemi-Lumi One L kit (Nacalai Tesque) or a Chemi-Lumi One Super kit (for Figure 5S only) and images were captured with the Amersham ImageQuant 800 (Cytiva).

Establishment of BROMI-KO and FAM149B1-KO cells

Disruption of the *BROMI* and *FAM149B1* genes in hTERT-RPE1 cells by the CRISPR/Cas9 system using homology-independent DNA repair was carried out as described previously (Katoh *et al.*, 2017), with some modifications (Okazaki *et al.*, 2020; Fujisawa *et al.*, 2021). Briefly, single-guide RNA (sgRNA) sequences targeting the human *BROMI/TBC1D32* or *FAM149B1* gene (see Supplemental Table S3) were designed using CRISPOR (Haeussler *et al.*, 2016). Double-stranded oligonucleotides for the target sequences were inserted into the all-in-one sgRNA expression vector, pHiFiCas9-2 × sgRNA (Addgene 162277) (Fujisawa *et al.*, 2021). hTERT-RPE1 cells seeded on a 12-well plate to approximately 1.5×10^5 cells, and the next day they were transfected with the all-in-one vector and the donor knock-in vector, pDonor-tBFP-NLS-Neo(universal) (Addgene 80767) (Katoh *et al.*, 2017), using X-tremeGENE9 Reagent (Roche Applied Science). After selection of the transfected cells in the presence of G418 (600 µg/ml), cells were isolated using an SH800 cell sorter (SONY) at the Medical Research Support Center, Graduate School of Medicine, Kyoto University. Genomic DNA extracted from the isolated cells was analyzed by PCR using GoTaq Master Mixes (Promega) and PrimeSTAR GXL Premix Fast (Takara Bio) and three sets of primers (Supplemental Table S3) to distinguish the following three states of integration of the donor knock-in vector: forward integration (Supplemental Figure S2, A and C, b, b′), reverse integration (c, c′), and no integration with a small indel (a, a′). The disruption of both alleles of *BROMI* and *FAM149B1* was confirmed by direct sequencing of the PCR products.

The *ICK*-KO cell line #ICK-4-6 and the *CCRK*-KO cell line #CCRK-2-4 were established as described previously (Nakamura *et al.*, 2020; Noguchi *et al.*, 2021).

Preparation of cells stably expressing EGFP-fused BROMI, FAM149B1, and CFAP20 constructs

Lentiviral vectors for the expression of various BROMI and FAM149B1 constructs and a CFAP20 construct were prepared as described previously (Takahashi *et al.*, 2012). Briefly, pRRLsinPPT-EGFP-N-BROMI or its mutant, pRRLsinPPT-EGFP-N-FAM149B1 or its mutant, or pRRLsinPPT-EGFP-N-CFAP20 was transfected into HEK293T cells along with the packaging plasmids (pRSV-REV, pMD2.g, and pMDLg/pRRE [Thomas *et al.*, 2009] kindly provided by Peter McPherson, McGill University). Culture media were replaced 8 h after transfection, and those containing viral particles were collected at 24, 36, and 48 h after transfection. The collected media were passed through a 0.45-µm filter and centrifuged at 32,000 × *g* at 4°C for 4 h. The precipitates containing lentiviral particles were resuspended in Opti-MEM (Thermo Fisher). The preparation of lentiviral vectors for the ICK constructs was as described previously (Nakamura *et al.*, 2020; Noguchi *et al.*, 2021). The lentiviral suspension was added to the culture medium of hTERT-RPE1 cells or KO cell lines and used for subsequent analyses after a 24-h incubation.

Immunofluorescence analysis and live-cell imaging

hTERT-RPE1, *BROMI*-KO, *FAM149B1*-KO, *CCRK*-KO, and *ICK*-KO cells were cultured in DMEM/F-12 (Nacalai Tesque) supplemented with 10% FBS and 0.348% sodium bicarbonate. To induce ciliogenesis, the cells were grown on coverslips to 100% confluence and serum-starved for 24 h in DMEM/F-12 containing 0.2% bovine serum albumin.

Unless otherwise stated, immunofluorescence analysis was performed as described previously (Noguchi *et al.*, 2021; Zhou *et al.*, 2022). Briefly, cells on coverslips were fixed with 3% paraformaldehyde for 5 min at room temperature and permeabilized with 100% methanol for 5 min at –20°C (for experiments shown in Figures 2, P–R; 3, A–H; 4, A–P; and 7, A–E, H and I; and Supplemental Figure S1, B–G), fixed and permeabilized with 100% methanol for 5 min at –20°C (for experiments shown in Figures 2, A–L; and 5, A–O), and washed three times with phosphate-buffered saline. The fixed/permeabilized cells were blocked with 10% FBS, incubated sequentially with primary and secondary antibodies diluted in Can Get Signal Immunostain Solution A (Toyobo) (for the detection of SMO) or in 5% FBS (for the detection of the other proteins), and observed using an Axio Observer microscope (Carl Zeiss). A region of interest (ROI) was created by drawing a line of 3-point width along the signal of ARL13B or Ac-tubulin within cilia using a segmented line tool in the ZEN 3.1 imaging software (Carl Zeiss). For the correction of local background intensity, the ROI was duplicated and set to a nearby region. Statistical analyses were performed using JMP Pro 16 software (SAS Institute).

Live-cell imaging to observe the release of ECVs from cilia was performed as described previously (Nakamura *et al.*, 2020; Kobayashi *et al.*, 2021). Briefly, *BROMI*-KO cells expressing EGFP-fused ARL13B(ΔGD) were serum-starved for 24 h on a glass-bottom culture dish (MatTek) and observed under an A1R-MP confocal laser-scanning microscope (Nikon). Time-lapse images were acquired sequentially every 5 min and analyzed using NIS-Elements imaging software (Nikon).

ACKNOWLEDGMENTS

We thank Peter McPherson for kindly providing the lentiviral vectors, Takahisa Furukawa for kindly providing the ICK plasmids and Helena Akiko Popiel for critical reading of the manuscript. This work was supported in part by grants from the Japan Society for the Promotion of Science (JSPS) (Grants No. 19H00980 and No. 20H04904 to K.N. and No. 18H02403 and No. 21H02427 to Y.K.) and a grant of JRPs-LEAD with UKRI from the JSPS to K.N. (Grant No. JPJSJRP20181701).

REFERENCES

Adly N, Alhashem A, Ammari A, Alkuraya FS (2014). Ciliary genes *TBC1D32/C6orf170* and *SCLT1* are mutated in patients with OFD type IX. Hum Mut 35, 36–40.

Alsahan N, Alkuraya FS (2020). Confirming *TBC1D32*-related ciliopathy in humans. Am J Med Genet 182, 1985–1987.

Anvarian Z, Mykytyn K, Mukhopadhyay S, Pedersen LB, Christensen ST (2019). Cellular signaling by primary cilia in development, organ function and disease. Nat Rev Nephrol 15, 199–219.

Asleson CM, Lefebvre PA (1998). Genetic analysis of flagellar length control in *Chlamydomonas reinhardtii*: a new *long-flagella* locus and extragenic suppressor mutations. Genetics 148, 693–702.

Badgandi HB, Hwang S, Shimada IS, Loriot E, Mukhopadhyay S (2017). Tubby family proteins are adaptors for ciliary trafficking of integral membrane proteins. J Cell Biol 216, 743–760.

Bengs F, Scholz A, Kuhn D, Wiese M (2005). LmxMPK9, a mitogen-activated protein kinase homologue affects flagellar length in *Leishmania mexicana*. Mol Microbiol 55, 1606–1615.

Berman SA, Wilson NF, Haas NA, Lefebvre PA (2003). A novel MAP kinase regulates flagellar length in *Chlamydomonas*. Curr Biol 13, 1145–1149.

Bertiaux E, Mallet A, Fort C, Blisnick T, Bonnefoy S, Jung J, Lemos M, Marco S, Vaughan S, Trépout S, *et al*. (2018). Bidirectional intraflagellar transport is restricted to two sets of microtubule doublets in the trypanosome flagellum. J Cell Biol 217, 4284–4297.

Blomen VA, Májek P, Jae LT, Bigenzahn JW, Nieuwenhuis J, Staring J, Sacco R, van Diemen FR, Olk N, Stukalov A, *et al*. (2015). Gene essentiality and synthetic lethality in haploid human cells. Science 350, 1092–1096.

Boldt K, van Reeuwijk J, Lu Q, Koutroumpas K, Nguyen TM, Texier Y, van Beersum SEC, Horn N, Willer JR, Mans D, *et al*. (2016). An organelle-specific protein landscape identifies novel diseases and molecular mechanisms. Nat Commun 7, 11491.

Braun DA, Hildebrandt F (2017). Ciliopathies. Cold Spring Harb Perspect Biol 9, a028191.

Burghoorn J, Dekkers MPJ, Rademakers S, de Jong T, Willemsen R, Jansen G (2007). Mutation of the MAP kinase DYF-5 affects docking and undocking of kinesin-2 motors and reduces their speed in the cilia of *Caenorhabditis elegans*. Proc Natl Acad Sci USA 104, 7157–7162.

Chaya T, Furukawa T (2021). Post-translational modification enzymes as key regulators of ciliary protein trafficking. J Biochem 169, 633–642.

Chaya T, Omori Y, Kuwahara R, Furukawa T (2014). ICK is essential for cell type-specific ciliogenesis and the regulation of ciliary transport. EMBO J 33, 1227–1242.

Chien AS, Shih SM, Bower R, Tritschler D, Porter ME, Yildiz A. (2017). Dynamics of the IFT machinery at the ciliary tip. eLife 6, e28606.

Ding M, Jin L, Xie L, Park SH, Tong Y, Wu D, Chhabra AB, Fu Z, Li X (2018). A murine model for human ECO syndrome reveals a critical role of intestinal cell kinase in skeletal development. Calcif Tissue Int 102, 348–357.

Fu Z, Gailey CD, Wang EJ, Brautigan DL (2019). Ciliogenesis associated kinase 1 (CILK1): targets and functions in various organ systems. FEBS Lett 593, 2990–3002.

Fu Z, Larson KA, Chitta RK, Parker SA, Turk BE, Lawrence MW, Kaldis P, Galaktionov K, Cohn SM, Shabanowitz J, *et al*. (2006). Identification of yin-yang regulators and a phosphorylation consensus for male germ cell-associated kinase (MAK)-related kinase. Mol Cell Biol 26, 8639–8654.

Fu Z, Schroeder MJ, Shabanowitz J, Kaldis P, Togawa K, Rustgi AK, Hunt DF, Sturgill TW (2005). Activation of a nuclear Cdc2-related kinase within a mitogen-activated protein kinase-like TDY motif by autophosphorylation and cyclin-dependent protein kinase-activating kinase. Mol Cell Biol 25, 6047–6064.

Fujisawa S, Qiu H, Nozaki S, Chiba S, Katoh Y, Nakayama K (2021). ARL3 and ARL13B GTPases participate in distinct steps of INPP5E targeting to the ciliary membrane. Biol Open 10, bio058843.

Gailey CD, Wang EJ, Jin L, Ahmadi S, Brautigan DL, Li X, Xu W, Scott MM, Fu Z (2021). Phosphosite T674A mutation in kinesin family member 3A fails to reproduce tissue and ciliary defects characteristic of CILK1 loss of function. Dev Dyn 250, 263–273.

Garcia-Gonzalo FR, Reiter JF (2017). Open sesame: how transition fibers and the transition zone control ciliary composition. Cold Spring Harb Perspect Biol 9, a028134.

Haeussler M, Schönig K, Eckert H, Eschstruth A, Mianné J, Renaud JB, Schneider-Maunoury S, Shkumatava A, Teboul L, Kent J, *et al*. (2016). Evaluation of off-target and on-target scoring algorithms and integration into the guide RNA selection tool CRISPOR. Genome Biol 17, 148.

Hamada Y, Tsurumi Y, Nozaki S, Katoh Y, Nakayama K (2018). Interaction of WDR60 intermediate chain with TCTEX1D2 light chain of the dynein-2 complex is crucial for ciliary protein trafficking. Mol Biol Cell 29, 1628–1639.

Han S, Miyoshi K, Shikada S, Amano G, Wang Y, Yoshimura T, Katayama T (2019). TULP3 is required for localization of membrane-associated proteins ARL13B and INPP5E to primary cilia. Biochem Biophys Res Commun 509, 227–234.

Hietamäki J, Gregory LC, Ayoub S, Livonen T, Vaaralahti K, Liu X, Brandstack N, Buckton AJ, Laire T, Känsäkoski J, *et al*. (2020). Loss-of-function variants in TBC1D32 underlie syndromic hypopituitarism. J Clin Endocrinol Metab 105, 1748–1758.

Hirano T, Katoh Y, Nakayama K (2017). Intraflagellar transport-A complex mediates ciliary entry as well as retrograde trafficking of ciliary G protein-coupled receptors. Mol Biol Cell 28, 429–439.

Huttlin EL, Bruckner RJ, Paulo JA, Cannon JR, Ting L, Baltier K, Colby G, Gebreab F, Gygi MP, Parzen H, *et al*. (2017). Architecture of the human interactome defines protein communities and disease networks. Nature 545, 505–509.

Ishida Y, Kobayashi T, Chiba S, Katoh Y, Nakayama K (2021). Molecular basis of ciliary defects caused by compound heterozygous *IFT144/WDR19* mutations found in cranioectodermal dysplasia. Hum Mol Genet 30, 213–225.

Ishikawa H, Thompson J, Yates JR III, Marshall WF (2012). Proteomic analysis of mammalian primary cilia. Curr Biol 22, 414–419.

Jiang Y-Y, Maier W, Baumeister R, Minevich G, Joachimiak E, Wloga D, Ruan Z, Kannan N, Bocarro S, Bahraini A, *et al*. (2019). LF4/MOK and a CDK-related kinase regulate the number and length of cilia in Tetrahymena. PLoS Genet 15, e1008099.

Jordan MA, Diener DR, Stepanek L, Pigino G (2018). The cryo-EM structure of intraflagellar transport trains reveals how dynein is inactivated to ensure unidirectional anterograde movement in cilia. Nat Cell Biol 20, 1250–1255.

Katoh Y, Michisaka S, Nozaki S, Funabashi T, Hirano T, Takei R, Nakayama K (2017). Practical method for targeted disruption of cilia-related genes by using CRISPR/Cas9-mediated homology-independent knock-in system. Mol Biol Cell 28, 898–906.

Katoh Y, Nakamura K, Nakayama K (2018). Visible immunoprecipitation (VIP) assay: a simple and versatile method for visual detection of protein-protein interactions. Bio-protocol 8, e2687.

Katoh Y, Nozaki S, Hartanto D, Miyano R, Nakayama K (2015). Architectures of multisubunit complexes revealed by a visible immunoprecipitation assay using fluorescent fusion proteins. J Cell Sci 128, 2351–2362.

Khalifa AAZ, Ichikawa M, Dai D, Kubo S, Black CS, Peri K, McAlear TS, Veyron S, Yang SK, Vargas J, *et al*. (2020). The inner junction complex of the cilia is an interaction hub that involves tubulin post-translational modifications. eLife 9, e52760.

Ko HW, Norman RX, Tran J, Fuller KP, Fukuda M, Eggenschwiler JT (2010). Broad-minded links cell cycle-related kinase to cilia assembly and Hedgehog signal transduction. Dev Cell 18, 237–247.

Kobayashi T, Ishida Y, Hirano T, Katoh Y, Nakayama K (2021). Cooperation of the IFT-A complex with the IFT-B complex is required for ciliary retrograde protein trafficking and GPCR import. Mol Biol Cell 32, 45–56.

Kopinke D, Norris AM, Mukhopadhyay S (2021). Developmental and regenerative paradigms of cilia regulated hedgehog signaling. Sem Cell Dev Biol 110, 89–103.

Lahiry P, Wang B, Robinson JF, Turowec JP, Litchfield DW, Lanktree MB, Gloor GB, Puffenberger EG, Strauss KA, Martens MB, *et al*. (2009). A multiplex human syndrome implicates a key role for intestinal cell kinase in development of central nervous, skeletal, and endocrine systems. Am J Hum Genet 84, 134–147.

Laligné C, Klotz C, de Loubresse NG, Lemullois M, Hori M, Laurent FX, Papon JF, Louis B, Cohen J, Koll F (2010). Bug22p, a conserved centrosomal/ciliary protein also present in higher plants, is required for an effective ciliary stroke in *Paramecium*. Euk Cell 9, 645–655.

Li D, Liu Y, Yi P, Zhu Z, Li W, Zhang QC, Li JB, Ou G (2021). RNA editing restricts hyper active ciliary kinases. Science 373, 984–991.

Li X, Wang W, Wang J, Malovannaya A, Xi Y, Li W, Guerra R, Hawke DH, Qin J, Chen J (2015). Proteomic analyses reveal distinct chromatin-associated and soluble transcription factor complexes. Mol Syst Biol 11, 775.

Liu P, Lechtreck KF (2018). The Bardet-Biedl syndrome protein complex is an adaptor expanding the cargo of range of intraflagellar transport trains for ciliary export. Proc Natl Acad Sci USA 115, E934–E943.

Liu Y-X, Xue B, Sun W-Y, Wingfield JL, Sun J, Wu M, Lechtreck KF, Wu Z, Fan Z-C (2021). Bardet-Biedl syndrome 3 protein promotes ciliary exit of the signaling protein phospholipase D via the BBSome. eLife 10, e59119.

Ma M, Stoyanova M, Rademacher G, Dutcher SK, Brown A, Zhang R (2019). Structure of the decorated ciliary doublet microtubule. Cell 179, 909–922.
Maia TM, Gogendeau D, Pennetier C, Janke C, Basto R (2014). Bug22 influences cilium morphology and the post-translational modification of ciliary microtubules. Biol Open 3, 138–151.
Malumbres M (2014). Cyclin-dependent kinases. Genome Biol 15, 122.
Maurya AK, Rogers T, Sengupta P (2019). A CCRK and a MAK kinase modulate cilia branching and length via regulation of axonemal microtubule dynamics in *Caenorhabditis elegans*. Curr Biol 29, 1286–1300.
Maurya AK, Sengupta P (2021). *xbx-4*, a homolog of the Joubert syndrome gene *FAM149B1*, acts via the CCRK and RCK kinase cascade to regulate cilia morphology. Curr Biol 31, 5642–5649.
Meng D, Cao M, Oda T, Pan J (2014). The conserved ciliary protein Bug22 controls planar beating of *Chlamydomonas* flagella. J Cell Sci 127, 281–287.
Mijalkovic J, van Krugten J, Oswald F, Acar S, Peterman EJG (2018). Single-molecule turnarounds of intraflagellar transport at the *C. elegans* ciliary tip. Cell Rep 25, 1701–1707.
Moon H, Song J, Shin J-O, Lee H, Kim H-K, Eggenschwiler JT, Bok J, Ko HW (2014). Intestinal cell kinase, a protein associated with endocrine-cerebro-osteodysplasia syndrome, is a key regulator of cilia length and Hedgehog signaling. Proc Natl Acad Sci USA 111, 8541–8546.
Mukhopadhyay S, Wen X, Chih B, Nelson CD, Lane WS, Scales SJ, Jackson PK. (2010). TULP3 bridges the IFT-A complex and membrane phosphoinositides to promote trafficking of G protein-coupled receptors into primary cilia. Genes Dev 24, 2180–2193.
Nachury MV, Mick DU. (2019). Establishing and regulating the composition of cilia for signal transduction. Nat Rev Mol Cell Biol 20, 389–405.
Nakamura K, Noguchi T, Takahara M, Omori Y, Furukawa T, Katoh Y, Nakayama K (2020). Anterograde trafficking of ciliary MAP kinase-like ICK/CILK1 by the intraflagellar transport machinery is required for intraciliary retrograde protein trafficking. J Biol Chem 295, 13363–13376.
Nakayama K, Katoh Y (2020). Architecture of the IFT ciliary trafficking machinery and interplay between its components. Crit Rev Biochem Mol Biol 55, 179–196.
Nievergelt AP, Zykov I, Diener D, Buchholz T-O, Delling M, Diez S, Jug F, Štěpánek L, Pigino G (2021). Intraflagellar transport trains can turn around without the ciliary tip complex. bioRxiv doi: https://doi.org/10.1101/2021.1103.1119.436138.
Nishijima Y, Hagiya Y, Kubo T, Takei R, Katoh Y, Nakayama K (2017). RABL2 interacts with the intraflagellar transport B complex and CEP19 and participates in ciliary assembly. Mol Biol Cell 28, 1652–1666.
Noguchi T, Nakamura K, Satoda Y, Katoh Y, Nakayama K (2021). CCRK/CDK20 regulates ciliary retrograde protein trafficking via interacting with BROMI/TBC1D32. PLoS ONE 16, e0258497.
Nozaki S, Castro Araya RF, Katoh Y, Nakayama K (2019). Requirement of IFT-B–BBSome complex interaction in export of GPR161 from cilia. Biol Open 8, bio043786.
Nozaki S, Katoh Y, Kobayashi T, Nakayama K (2018). BBS1 is involved in retrograde trafficking of ciliary GPCRs in the context of the BBSome complex. PLoS ONE 13, e0195005.
Oh YS, Wang EJ, Gailey CD, Brautigan DL, Allen BL, Fu Z (2019). Ciliopathy-associated protein kinase ICK requires its non-catalytic carboxyl-terminal domain for regulation of ciliogenesis. Cells 8, 677.
Okamoto S, Chaya T, Omori Y, Kuwahara R, Kubo S, Sakaguchi H, Furukawa T (2017). Ick ciliary kinase is essential for planar cell polarity formation in inner ear hair cells and hearing function. J Neurosci 37, 2073–2085.
Okazaki M, Kobayashi T, Chiba S, Takei R, Liang L, Nakayama K, Katoh Y (2020). Formation of the B9-domain protein complex MKS1–B9D2–B9D1 is essential as a diffusion barrier for ciliary membrane proteins. Mol Biol Cell 31, 2259–2268.
Omori Y, Chaya T, Katoh K, Sato S, Muraoka K, Ueno S, Koyasu T, Kondo M, Furukawa T (2010). Negative regulation of ciliary length by ciliary male germ cell-assoaciated kinase (Mak) is required for retinal photoreceptor survival. Proc Natl Acad Sci USA 107, 22671–22676.
Oud M, Bonnard C, Mans D, Altunoglu U, Tohari S, Ng A, Eskin A, Lee H, Rupar C, de Wagenaar N, *et al*. (2016). A novel ICK mutation causes ciliary disruption and lethal endocrine-cerebro-osteodysplasia syndrome. Cilia 5, 8.
Picariello T, Brown JM, Hou Y, Swank G, Cochran DA, King OD, Lechtreck K, Pazour GJ, Witman GB (2019). A global analysis of IFT-A function reveals specialization for transport of membrane-associated proteins into cilia. J Cell Sci 132, jcs220749.
Reiter JF, Leroux MR (2017). Genes and molecular pathways underpinning ciliopathies. Nat Rev Mol Cell Biol 18, 533–547.
Shaheen R, Jiang N, Alzahrani F, Ewida N, Al-Sheddi T, Alobeid E, Musaev D, Stanley V, Hashem M, Ibrahim N, *et al*. (2019). Bi-allelic mutations in *FAM149B1* cause abnormal primary cilium and a range of ciliopathy phenotypes in humans. Am J Hum Genet 104, 731–737.
Siegert S, Mindler GT, Brücke C, Kranzl A, Patsch J, Ritter M, Janecke AR, Vodopiutz J (2021). Expanding the phenotype of the *FAM149B1*-related ciliopathy and identification of three neurogenetic disorders in a single family. Genes 12, 1648.
Snouffer A, Brown D, Lee H, Walsh J, Lupu F, Norman R, Lechtreck K, Ko HW, Eggenschwiler J (2017). Cell cycle-related kinase (CCRK) regulates ciliogenesis and Hedgehog signaling in mice. PLoS Genet 13, e1006912.
Stepanek L, Pigino G (2016). Microtubule doublets are double-track railways for intraflagellar transport trains. Science 352, 721–724.
Takahashi S, Kubo K, Waguri S, Yabashi A, Shin H-W, Katoh Y, Nakayama K (2012). Rab11 regulates exocytosis of recycling vesicles at the plasma membrane. J Cell Sci 125, 4049–4057.
Tam L-W, Wilson NF, Lefebvre PA (2007). A CDK-related kinase regulates the length and assembly of flagella in *Chlamydomonas*. J Cell Biol 176, 819–829.
Taschner M, Lorentzen E (2016). The intraflagellar transport machinery. Cold Spring Harb Perspect Biol 8, a028092.
Taylor SP, Bosakova MK, Varecha M, Balek L, Barta T, Trantirek L, Jelinkova I, Duran I, Vesela I, Forlenza KN, *et al*. (2016). An inactivating mutation in intestinal cell kinase, ICK, impairs hedgehog signalling and causes short rib-polydactyly syndrome. Hum Mol Genet 25, 3998–4011.
Thomas S, Ritter B, Verbich D, Sanson C, Bourbonnière L, McKinney RA, McPherson PS (2009). Intersectin regulates dendritic spine development and somatodendritic endocytosis but not synaptic vesicle recycling in hippocampal neurons. J Biol Chem 284, 12410–12419.
Toropova K, Zalyte R, Mukhopadhyay AG, Mladenov M, Carter AP, Roberts AJ (2019). Structure of the dynein-2 complex and its assembly with intraflagellar transport trains. Nat Struct Mol Biol 26, 823–829.
Tunyasuvunakool K, Adler J, Wu Z, Green T, Zielinski M, Žídek A, Bridgland A, Cowie A, Meyer C, Laydon A, *et al*. (2021). Highly accurate protein structure prediction for the human proteome. Nature 596, 590–596.
Wang C, Li J, Takemaru K, Jiang X, Xu G, Wang B. (2018). Centrosomal protein Dzip1l binds Cby, promotes ciliary bud formation, and acts redundantly with Bromi to regulate ciliogenesis in the mouse. Development 145, dev164236.
Wang T, Birsoy K, Hughes NW, Krupczak KM, Post Y, Wei JJ, Lander ES, Sabatini DM (2015). Identification and characterization of essential genes in the human genome. Science 350, 1096–1101.
Wang Y, Ren Y, Pan J (2019). Regulation of flagellar assembly and length in *Chlamydomonas* by LF4, a MAPK-related kinase. FASEB J 33, 6431–6441.
Wingfield JL, Mekonnen B, Mengoni I, Liu P, Jordan M, Diener D, Pigino G, Lechtreck K (2021). In vivo imaging shows continued association of several IFT A, B and dynein complexes while IFT trains U-turn at the tip. J Cell Sci 134, jcs259010.
Yanagisawa H, Mathis G, Oda T, Hirono M, Richey EA, Ishikawa H, Marshall WF, Kikkawa M, Qin H (2014). FAP20 is an inner junction protein of doublet microtubules essential for both the planar asymmetrical waveform and stability of flagella in *Chlamydomonas*. Mol Biol Cell 25, 1472–1483.
Yang Y, Roine N, Mäkelä TP (2013). CCRK depletion inhibits glioblastoma cell proliferation in a cilium-dependent manner. EMBO Rep 14, 741–747.
Ye F, Nager AR, Nachury MV (2018). BBSome trains remove activated GPCRs from cilia by enabling passage through the transition zone. J Cell Biol 217, 1847–1868.
Yi P, Xie C, Ou G (2018). The kinases male germ cell-associated kinase and cell cycle-related kinase regulate kinesin-2 motility in *Caenorhabditis elegans* neuronal cilia. Traffic 19, 522–535.
Zhou Z, Qiu H, Castro-Araya R-F, Takei R, Nakayama K, Katoh Y (2022). Impaired cooperation between IFT74/BBS22–IFT81 and IFT25–IFT27/BBS19 in the IFT-B complex causes ciliary defects in Bardet-Biedl syndrome. Hum Mol Genet 31, ddab354.